

RESEARCH ARTICLE

New insight into the coloration mechanism and synthesis of ultrafine Pr-ZrSiO₄ yellow pigments

Shan Peng^{1,#} | Ranran Yang^{1,#} | Binglong Lei^{1,2}  | Renhua Chen² | Yun Gao¹ | Xiaohong Xia¹ | Kevin P. Homewood¹

¹Hubei Collaborative Innovation Center for Advanced Organic Chemical Materials, Ministry-of-Education Key Laboratory for the Green Preparation and Application of Functional Materials, School of Materials Science and Engineering, Hubei University, Wuhan, China

²Jinhuan Pigments Co. Ltd., Yichun, China

Correspondence

Binglong Lei and Yun Gao, Hubei Collaborative Innovation Center for Advanced Organic Chemical Materials, Ministry-of-Education Key Laboratory for the Green Preparation and Application of Functional Materials, School of Materials Science and Engineering, Wuhan, 430062 Hubei, China.

Email: lei@hubu.edu.cn;
gaoyun@hubu.edu.cn

Funding information

National Natural Science Foundation of China, Grant/Award Numbers: 51602096, 12174092, 11874144, 21801071; China Postdoctoral Science Foundation, Grant/Award Number: 2020M682382; Hubei Provincial Department of Science and Technology, Grant/Award Numbers: 2018CFA026, 2019CFA079; Wuhan Science and Technology Bureau, Grant/Award Number: 2018010401011268; Program of Introducing Talents of Discipline to Universities, Grant/Award Number: D18025

Abstract

It is of particular significance to unveil the authentic coloration mechanism of the multivalent praseodymium colored ZrSiO₄ yellow pigments for advanced decoration applications. We herein adopted a facile strategy to modulate the fluorine-assisted zircon crystallization and thereby obtained ultrafine Pr-ZrSiO₄ yellow pigments, which have a remarkably narrow size distribution and average diameters within 250–400 nm. By virtue of some cogent combinative spectra of reflection, absorption, excitation, and emission from three types of elaborately-designed H₂-, air-, and O₂-based pigments, the coloration mechanism for the Pr-colored zircon was systematically unveiled: both Pr⁴⁺ and Pr³⁺ coexist invariably in the pigments, while the former contributes primarily to the ligand-to-metal charge transfer from O_{2p} to Pr(IV)_{4f} for the blue–violet absorption to generate the yellow hue, and the latter is inclined to discolor the pigments. Therefore, an oxidizing atmosphere is preferable to produce brilliant Pr-ZrSiO₄ pigments with enhanced chromatic properties. The stark spectroscopic distinctions between the wide-band absorption from the nonluminescent tetravalency and the narrow-band absorption from the luminescent trivalency can expand our understanding to the rare-earth-based inorganic pigments.

KEYWORDS

luminescence, mechanism, morphology, pigment, spectroscopy, zircon

1 | INTRODUCTION

The praseodymium-doped zircon yellow pigments (Pr-ZrSiO₄), as one of the very few high-temperature inorganic pigments, are widely applied in conventional inorganic decoration and also the high-tech digital print-

ing for their environmental benignity, superb yellowish hues, outstanding chemical/thermal stability and desirable compatibility with other pigments and ceramic bodies.^{1–4} However, the Pr-ZrSiO₄ pigments, as naturally allochromatic pigments, are still inferior in the tinting strength (the colorimetric values $b^* = 45–82$, typically $50–65$)^{3–6} to those idiochromatic pigments (such as BiVO₄ and CdS_{1-x}S_x, with b^* as high as 92–99).^{7–10} It is still

[#]Shan Peng and Ranran Yang contributed equally to this work.

challenging the researchers to further promote these pigments to a higher coloring performance in both the micron-sized ones for conventional applications and also the submicron-sized ultrafine powders for the thriving high-tech digital decoration.¹ From long-term perspectives, a central question is still open whether or not one can transform these pigments into some suprapigments (with the chroma value C^* exceeding 100, defined in the authors' work to be unpublished) for more advanced applications.

Of the first and foremost significance is to determine the real provenance and also the hinderance of the yellow hue of the Pr-ZrSiO₄ pigments, which will be proven substantially valuable to promote the in-depth development for more rare-earth substituted pigments akin to these Pr-based pigments. The coloration mechanism has diverged throughout the process of research and application for the Pr-ZrSiO₄ pigments. One school argues that the yellow hue originates from the electronic $4f-4f$ transition within Pr³⁺,^{11,12} which explicitly cannot support the commonly high color saturation of the yellow hues in the pigments due to the naturally weak absorption from the $4f-4f$ transition. Another is inclined to attribute the coloration to the strong selective absorption in partial visible lights from the ligand-to-metal charge transfer (LMCT) from Pr⁴⁺ or to some other unclearly-explored reasons.¹³⁻¹⁵ Obviously, there are no really cogent and multidimensional consolidations to support the latter views, since the characteristic photoluminescence in the Pr-ZrSiO₄ pigments invariably exists, and it must derive from Pr³⁺ rather than Pr⁴⁺. Indeed, it is difficult to determine the real chromatic function of praseodymium in the pigments, especially when its tetravalency and trivalency constantly coexist, and only one was often erroneously recognized present in the hybrid pigmental system. Convincible and reliable proofs are still anticipated to reveal the authentic coloration mechanism for these pigments.

Another concern relates to the synthesis of well-crystallized Pr-ZrSiO₄ pigments, which have an ideal submicron dimension of about 200–400 nm (just half the wavelength of visible lights) for maintaining the sufficient molten-glaze stability and also for the improved chromatic property from the enhanced light scattering and absorption-reflection. Furthermore, submicron pigments with a well-defined morphology give more favorable fluidity when applied in inkjet printing than most of sub-optimal colorants with an irregular morphology and wide size distribution. It is to date still a challenge to fulfill these requirements via a facile solid-state reaction synthesis, since the robust ZrSiO₄ matrix gets crystallized only at high temperatures, typically over 1000°C, which usually induces severely aggregated large particles with average sizes up to 3–20 μm and a wide size distribution.^{2,11,16-19} In

contrast, a low-temperature hydrothermolysis can indeed realize uniform or even monodisperse zircon powders at only 150–370°C,^{20,21} but these liquid-based preferentially-grown zircons have little encapsulation capability to any heterogenic cations or particulate chromophores (like CdS_{1-x}Se_x and Fe₂O₃); therefore, hydrothermolysis was typically applied for the precursor treatment and often followed by a high-temperature calcination.²² Alternatively, a top-down route is generally applied to pulverize the conventional micron-sized pigments into submicron powders,¹⁷ which consumes much energy and, however, produces the pigments with suboptimal crushed particles.

Herein, we synthesized ultrafine Pr-ZrSiO₄ yellow pigments via a facile one-step route and explored of the origin of their yellow hues. Ammonium fluoride (NH₄F) as an effective formation inhibitor was introduced into the acidic reactive environment to control the growth-aggregation process of the zircon crystals. By varying the calcination atmospheres (H₂, O₂, N₂, and air), the pigments were modulated with distinct spectroscopic performance. These preconditions enable us to determinate the real hue provenance for the Pr-ZrSiO₄ pigments. This work provides some new insights into the coloring mechanism of the rare-earth-based pigments.

2 | EXPERIMENTAL

2.1 | Materials

Zirconium oxychloride (ZrOCl₂·8H₂O), sodium metasilicate (Na₂SiO₃·9H₂O), zinc oxide (ZnO), glycol, sodium fluoride (NaF), ammonium fluoride (NH₄F), and sodium chloride (NaCl) were of analytical grade and applied without further purification. Hydrochloric acid (HCl, 36.5 wt%) and ammonia hydroxide (NH₃·H₂O, 25–28%) or their diluted solutions were adopted for pH regulation. All the reagents above were purchased from Sinopharm Chemical Reagent (Shanghai, China). Analytical-grade praseodymium nitrate (Pr(NO₃)₃·6H₂O) was obtained from Aladdin Reagent (Shanghai, China). Deionized ultrapure water (18.25 MΩ, trace metals < 1 ppm) was prepared by a laboratory water purifier.

2.2 | Synthesis of Pr-ZrSiO₄ pigments

Ultrafine Pr-ZrSiO₄ pigments were synthesized by a coprecipitation method. Typically, ZrOCl₂·8H₂O (32.22 g, 0.1 mol) was dissolved in 100 mL deionized water, and Pr(NO₃)₃·6H₂O were added to obtain Pr/Zr mole ratios at 0 (labeled as Pr0), 2% (Pr2), 4% (Pr4), 6% (Pr6), 8% (Pr8), and 10% (Pr10), respectively. The pH value was adjusted to

4.0 with dilute $\text{NH}_3 \cdot \text{H}_2\text{O}$ (4.5 M). $\text{Na}_2\text{SiO}_3 \cdot 9\text{H}_2\text{O}$ (34.08 g, 0.12 mol) was then dissolved in 100 mL deionized water, and the pH was adjusted to 4.0 with dilute HCl (2.9 M). The two colloidal sols above were simultaneously pumped into another 100 mL NH_4F solution (2 mol/L, for F/Zr = 2.0 in mole) under vigorous stirring at room temperature, while pH of the mixed sol was maintained at 4.0. After heating in a water bath at 80°C for 4 h and aging for 12 h at room temperature, the suspension was filtered and washed with ultrapure water several times, and then dried at 120°C for 12 h to obtain a precursor powder. Subsequently, the precursor xerogel was calcinated at 950°C for 1 h after addition of 5.0 wt% NaF and 10 wt% NaCl as mixture mineralizers, and final pigments were obtained after acid washing (via 4.0 mol/L HNO_3) and drying at 120°C overnight. The normal zircon was similarly synthesized without addition of NH_4F and a Pr source (see the [supporting file](#)).

To explore the coloration mechanism of the Pr-ZrSiO₄ pigments, different calcination atmospheres were applied: the precursor powders were calcinated at 950°C for 1 h (heat ramp rate of $5^\circ\text{C}/\text{min}$) under the atmospheres of H₂ (5% in N₂), air and pure O₂. The pigments are denoted as H₂-based Pr6, air-based Pr6, and O₂-based Pr6, respectively. To optimize the tinting strength, ZnO was additionally applied in the mixed precursor to produce the pigments of P6Z0–5 (Table S1).

2.3 | Characterization

Crystalline phases of the Pr-ZrSiO₄ pigments were determined by X-ray diffraction (XRD, D8 Advance, Bruker) with a Cu $K_{\alpha 1}$ radiation source ($\lambda = 1.54056 \text{ \AA}$) at 40 kV and 40 mA in the scan range of $10\text{--}60^\circ$ at a scanning rate of $0.02^\circ/\text{s}$. The X-ray diffraction data were analyzed by Rietveld refinement using the TOPAS software (Version 6.0). The morphology of pigments was scanned using a field-emission scanning electron microscope (JSM-7100F, JEOL). The particle size distribution of Pr-ZrSiO₄ pigments was obtained by a laser particle size analyzer (ZS90, Malvern, UK). The chemical composition and element contents were performed by X-ray photoelectron spectroscopy (XPS, ESCALAB 250Xi) and energy-dispersive spectrum (EDS) (Bruker, Flash6 XFlash 6I30). Reflectance spectra of pigments were measured by a spectroscope (UV-2450, Shimadzu, Japan) in the wavelength range of 300–700 nm. The chromatic properties of pigments were tested according to the CIE system by a chromometer (YS30, 3NH); the parameter L^* represents the lightness, a^* the hue level of red to green and b^* the hue level of blue to yellow. The parameter C^* (chroma) represents the color saturation

and defined as $C^* = \sqrt{(a^*)^2 + (b^*)^2}$. The excitation (photoluminescence excitation, PLE) and emission spectra (photoluminescence, PL) were collected on a Xe light (FLS980, Edinburgh) over 200–800 nm.

The density function theory (DFT) calculations were performed by the Vienna ab initio simulation package. The projector-augmented-wave method was used to describe the ion–electron interactions, and the Perdew–Burke–Ernzerhof and generalized gradient approximation were applied for the exchange–correlation functional to treat the interactions between electrons. To include the Van der Waals interactions, the Grimme D3 dispersion correction was utilized. The DFT+U approach was used to handle the highly correlated 3d and 4f electrons, and U values of 7.0 and 6.335 eV were used for Zr and Pr, respectively. Considering the 3d orbital of Zn as a full one, U was not applied for the Zn atom. Tetragonal ZrSiO₄ has a space group of $I4_1/amd$, and Zr and Si are located at the Wyckoff positions 4a and 4b, respectively, whereas O is set at the 16 h position. A unit cell of ZrSiO₄ containing 24 atoms is used in our calculations. The co-doping was simulated by substituting the Zr atoms with Pr and Zn. A plane-wave cutoff of 500 eV was used for the kinetic energy. A uniform Γ -centered Monkhorst–Pack k-point grid of $9 \times 9 \times 9$ was used for the Brillouin zone integrations. The energy convergence threshold of structural relaxation and geometry optimization was 10^{-6} eV. All atoms in the unit cell were fully relaxed without any symmetry constraints until the force on each atom was less than 0.01 eV/\AA .

3 | RESULTS AND DISCUSSION

3.1 | Basic traits of ultrafine Pr-ZrSiO₄ pigments

The crystalline status of the ultrafine Pr-ZrSiO₄ pigments, synthesized under a fluorine-rich acidic environment (pH = 4.0), is presented in Figure 1(A–B), Table 1, and Figure S1. After the calcination at 950°C for 2 h, all the colored pigments Pr2–Pr10 and the control pure zircon powders (Pr0 and the normal zircon) exhibit sufficient crystallization and have the main phase of tetragonal ZrSiO₄ and a minor phase of monoclinic ZrO₂ (m-ZrO₂). A small amount of ZrO₂ in most of the pigments usually cannot be removed even though an excess of silicon was initially introduced, or a prolonged calcination over 2 h was applied. As the Pr content increases from zero to 10%, the (200) diffraction peak is shifted slightly toward smaller angles [Figure 1(B)], which is consistent with the previous observations in Pr-ZrSiO₄ pigments³; while the lattice

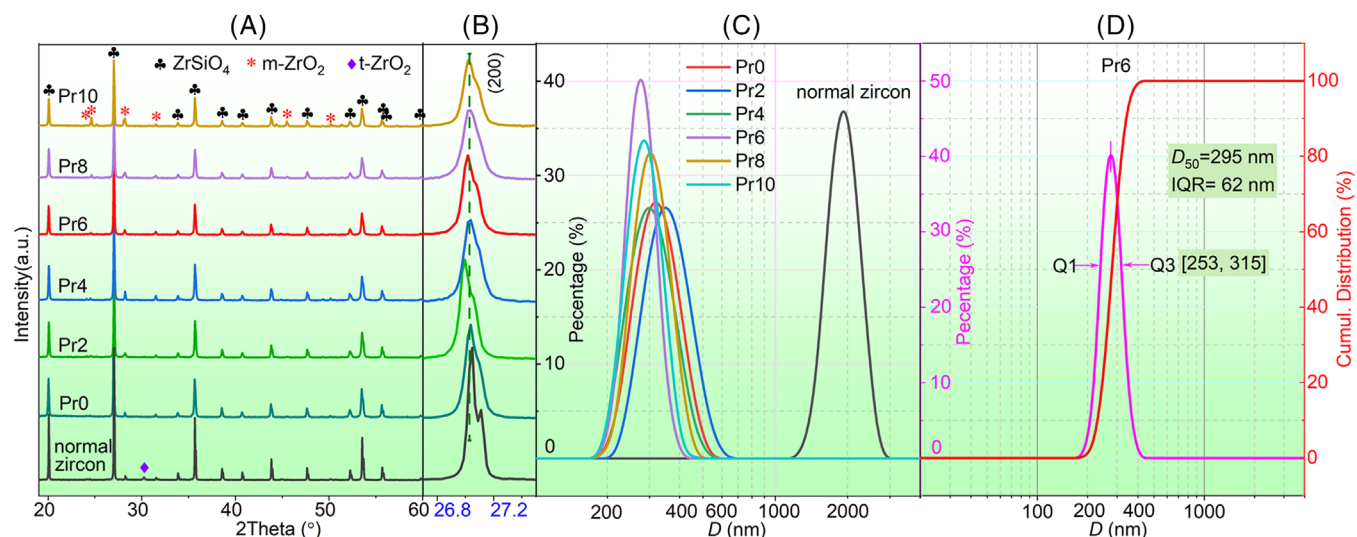


FIGURE 1 (A) X-ray diffraction (XRD) patterns of the ultrafine Pr-ZrSi₄ pigments of Pr0–Pr10 and the normal zircon; (B) the magnified patterns around $2\theta = 27^\circ$; (C and D) the size distribution of Pr0–Pr10 and the normal-zircon.

TABLE 1 Rietveld refinement results and the size information for Pr0–Pr10 and the normal zircon.

Sample	<i>a</i> (Å)	<i>c</i> (Å)	<i>V</i> (Å ³)	ZrSiO ₄ (mol %)	m-ZrO ₂ (mol %)	[Q1, Q3] (nm)	IQR (nm)	<i>D</i> ₅₀ (nm)
Pr0	6.6035(7)	5.9783(5)	260.69(8)	96.77	3.23	[288, 394]	106	338
Pr2	6.6040(6)	5.9797(4)	260.79(6)	94.00	6.00	[312, 438]	126	367
Pr4	6.6045(5)	5.9803(0)	260.86(4)	89.60	10.40	[271, 373]	102	317
Pr6	6.6047(9)	5.9803(0)	260.87(7)	88.02	11.98	[253, 315]	62	283
Pr8	6.6048(6)	5.9804(6)	260.89(7)	82.28	17.72	[278, 357]	79	313
Pr10	6.6040(4)	5.9803(2)	260.85(0)	69.10	30.90	[258, 331]	73	292
normal zircon	6.6102(6)	5.9860(4)	261.56(6)	–	–	[1746, 2189]	443	1978

Note: IQR, interquartile range (see Figure S2). The numbers in brackets refer to the experimental uncertainty.

parameters *a* and *c* determined by the Rietveld refinement increase from 6.6035 to 6.6048 Å and from 5.9783 to 5.9804 Å, respectively, corresponding to the unit cell expansion from 260.69 to 260.85 Å³. This is attributed to the octa-coordinated replacement of mainly the larger Pr⁴⁺ (0.96 Å in radius) and partially Pr³⁺ (1.13 Å) for the smaller Zr⁴⁺ (0.84 Å).¹³ Explicitly, it is more difficult for Pr³⁺ than Pr⁴⁺ to replace the smaller Zr⁴⁺ in terms of both the requirements of comparable atom sizes and charge equilibrium.

Figures 1C,D and 2 present the size distribution and morphology of Pr2–Pr10 and the reference zircons (Pr0 and the normal zircon). All the zircon and pigments exhibit a morphology of well-defined submicron polyhedrons (fully- or partially- grown tetragonal-dipyramid) and have a very narrow size distribution over 200–500 nm, typically having the interquartile ranges (IQRs, defined in Figure S2) within 250–400 nm (shown in Table 1), which dwells well in half of the visible light range of 380–780 nm for enhanced light scattering. Among the pigments, Pr6 has the narrowest IQR of only 65 nm and, most importantly, a very desirable average size of *D*₅₀ = 295 nm, just within half

of the yellow-light wavelength range of 565–600 nm. In contrast, the pure normal zircon synthesized without the NH₄F inhibitor possesses average sizes of *D*₅₀ = 1.95 μm and irregular aggregated particles (Figure 2I), while the zircons or pigments obtained from basic precursors (pH = ~8.0) were often produced with severe aggregation and micron-sized large crystals (exceeding 4–8 μm, see Figure S3). The suboptimal powders were frequently encountered in zircon materials and usually cannot be easily tackled when the solid-calcination synthesis was conducted at 700–1200°C.

Diffuse reflectance spectra and absorption spectra in the visible range for the ultrafine Pr-ZrSi₄ pigments are presented in Figure 3. The pigments exhibit high reflectance in the green-to-red range of 500–700 nm and gradually-intensified absorption in the complementary violet-to-blue region of 380–500 nm with Pr increasing, therefore generating a vivid yellow hue. All the spectra of Pr2–Pr10 and even the pigments synthesized under a strong O₂ atmosphere (discussed below in detail) equally have an absorption band around 591 nm (i.e., a pivotal

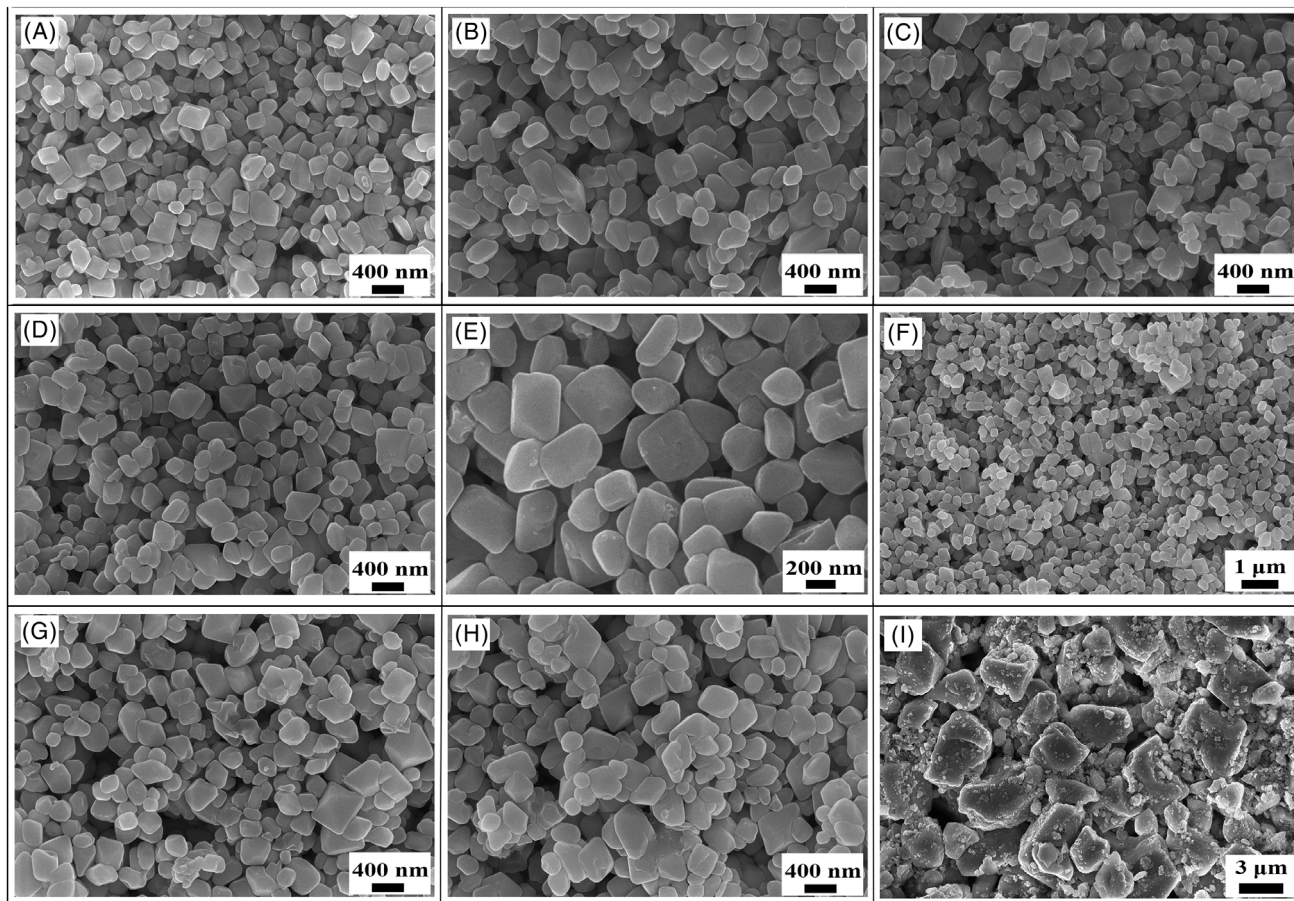


FIGURE 2 Scanning electron microscope (SEM) images of (A) Pr0, (B) Pr2, (C) Pr4, (D, E, and F) Pr6 at different magnifications, (G) Pr8, (H) Pr10, and (I) the normal zircon.

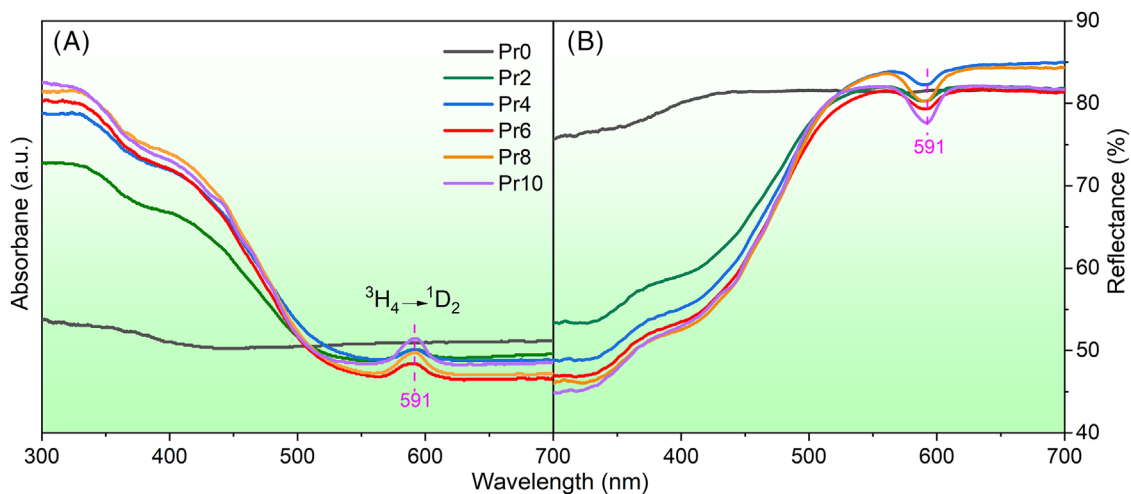


FIGURE 3 (A) The ultraviolet-visible (UV-VIS) absorption spectra, and (B) the diffuse reflectance spectra of Pr0–Pr10 synthesized in air.

contributing region for yellowness), which derives from the characteristic absorption of Pr^{3+} in the $4f-4f$ transition of ${}^3\text{H}_4 \rightarrow {}^1\text{D}_2$. All the Pr-ZrSiO₄ pigments in our work have unanimously maintained this characteristic

absorption band of Pr^{3+} , which was also observed by nearly all previous work ever reported,^{3,16,23,24} no matter what starting materials or synthetic routes were applied. This significant detail has failed to elicit the attention

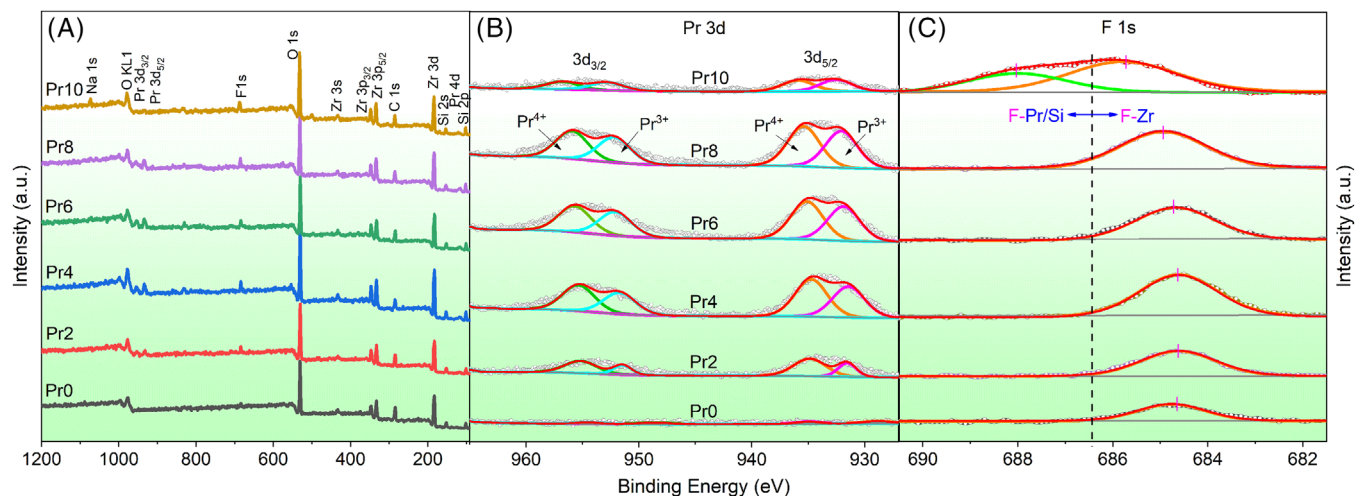


FIGURE 4 (A) Survey XPS spectra, and (B and C) the fine XPS spectra for Pr 3d and F 1s of Pr0–Pr10 synthesized in air.

TABLE 2 Chromatic parameters of Pr0–Pr10 sintered in air and the pigments sintered under the atmosphere of O₂ and H₂.

Sample	Pr/Zr (mol %)	F/Zr (mol %)	Chromaticity parameters			
			L*	a*	b*	C*
Pr0	1.78	22.77	95.84	0.15	1.75	1.76
Pr2	7.82	33.94	94.44	−2.99	13.07	13.41
Pr4	10.86	35.76	93.64	−3.02	15.37	15.66
Pr6	16.43	40.39	94.48	−3.54	17.57	17.92
Pr8	15.07	41.85	94.16	−3.78	17.10	17.51
Pr10	5.39	71.60	94.16	−4.24	17.08	17.59
Pr6-O ₂	–	–	91.14	−3.47	21.53	21.81
Pr6-H ₂	–	–	90.31	−1.38	4.24	4.46
Optimized Pr6-O ₂	–	–	85.25	−1.68	32.02	32.06

from most former researchers. It is safe to state that the Pr-ZrSiO₄ pigments must preserve the Pr cations at least partially in the trivalent state.

XPS spectra shown in Figure 4(A,B) further reveal the variation of Pr in the pigments, and the peaks around 955 and 935 eV correspond with the spin-orbit splitting of 3d_{3/2} and 3d_{5/2} of Pr. As the doping Pr increases nominally from 2% to 10%, the detected content ascends from 7.82% to 16.43% and then declines to 5.39% (Table 2 and Figure S4). The variation of the Pr content is roughly consistent with that obtained by EDS (Table S2). The content closely correlates with the yellowness index *b** and the chroma *C**, which respectively reach their maximum values of 17.57 and 17.92 around 6.0% and are then reduced at a higher Pr content. Further optimization can elevate the chroma *C** up to 32.02 by zinc doping (Table S1).

Here, the fluorine-controlled crystallization and growth (from acidic precursors, pH = 4.0) contribute primarily to the desirable advantages of the ultrafine Pr-ZrSiO₄ pigments: well-crystallized, nonaggregated, well-defined in

morphology and ultrafine in size, which usually cannot be met simultaneously in any zircon products via a single-step synthesis. In contrast, a few analogous Pr-ZrSiO₄ pigments can be synthesized but from some complex procedures (Table S3). A high-content growth inhibitor NH₄F (the F/Zr molar ratio 2.0) and the advantageous acidic precursors have jointly promoted these advantages. Fluorine in the acidic precursors can complex with Zr⁴⁺ more strongly than in neutral or basic solutions and even can generate the F/Zr ratios as high as 0.5–3 in final zircons (conversely, F/Zr = 0.3–0.8 in zircons synthesized at pH = 9.0); fluorine can be easily involved into the ZrSiO₄ network via the Zr species as Zr⁴⁺ + OH[−] + F[−] → Zr[(OH)_{1-x}·F_x]_n⁽⁴⁻ⁿ⁾⁺ in acidic solutions and even cannot be completely removed from the pigments after calcination at 900–1100°C.^{20,21} The fluoro-hydroxylated Zr complexes then react with the Si-OH species and the residual Zr-F terminals suppress the excessive extension of the Zr–O–Si bridging network in ZrSiO₄, hence reducing the size of final pigments. The F-induced growth also contributes to the Zr deficiency in the

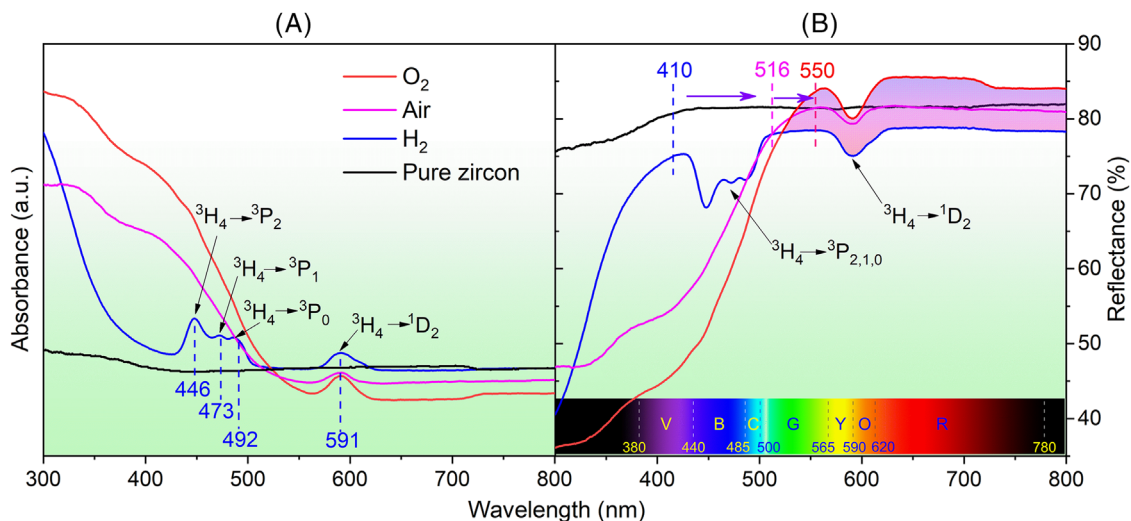


FIGURE 5 (A) UV-VIS absorption spectra, and (B) the diffuse reflectance spectra of Pr6 obtained under different atmospheres.

pigments (Si/Zr = 1.2–1.3, Figure S4), akin to that in the hydrothermal zircon products.²⁰ In contrast, the zircons or pigments, synthesized without NH_4F or from basic precursors (pH = ~ 8.0), can only be endowed with such desirable traits (Figure S3).

3.2 | Coloration mechanism of the Pr-ZrSiO₄ pigments

The coloration mechanism is further explored from some different perspectives, especially via the excitation and emission spectra simultaneously from three different types of pigments synthesized in the air, O₂, and H₂ atmospheres (referred to as Air-, O₂-, and H₂- based pigments, respectively). The distinctions of these pigments are presented in detail in terms of absorption/reflection, the electron binding analyses by XPS, theoretical calculation and the direct macroscopic visual appearance via the ultraviolet (UV) excitation and under the daylight.

The absorption–reflection spectra (Figure 5) and XPS data (Figure 6) present the difference of the three atmosphere-based pigments. As the oxidizing capability is intensified from H₂ to air and to O₂, the wide-band absorption onset shifts roughly from 410 to 550 nm, thereby generating the pigments varying in hue from nearly white ($b^* = 4.24$), to pale yellow ($b^* = 17.57$), and finally to favorable yellow ($b^* = 21.53$, in Table 2). In the pigments fabricated under the reducing H₂ atmosphere, most of the blue–violet lights cannot be absorbed, and they drastically dilute the yellowish hue, whereas the O₂-based pigments present a superior chroma over the air-based pigments.

For the first time, we observed the coexistence of the triple absorptive peaks of ${}^3\text{H}_4 \rightarrow {}^3\text{P}_{2,1,0}$ (446, 474, and 489 nm) and the peak of ${}^3\text{H}_4 \rightarrow {}^1\text{D}_2$ (591 nm) in the H₂-based

Pr-ZrSiO₄ pigments (Figure 5). Although the four narrow-band peaks equally belong to the $4f-4f$ transition of Pr³⁺, the first three peaks are often completely eclipsed by the much stronger wide-band absorption at 245–550 nm from the LMCT of O_{2p} → Pr(IV)_{2p} and they, therefore, cannot be observed in typical Pr-ZrSiO₄ pigments,^{3,12} whereas only the absorption at 591 nm remains the sole landmark for the existence of Pr³⁺ in all the pigments.^{1,16,23,24} The absorption below 410 nm in the H₂-based pigments is still attributed to the LMCT of O_{2p} → Pr(IV)_{2p} from the remaining Pr⁴⁺, without which the absorption onset continues to shift to only 225 nm in pure zircon (discussed in the end part). The $4f-4f$ transitions above generally belong to the partially-forbidden electric-dipole transitions, which often generate narrow-banded or quasi-lined absorption (often widened at room temperature, and typically with the absorption cross-sections below 10^{-20} cm² and absorption coefficients below 10^2 cm⁻¹),^{25–27} whereas the LMCT from oxygen to Pr⁴⁺ is intrinsically allowed and therefore generates a strong wide-band absorption (from 220 to 550 nm, with absorption coefficients over 10^4 cm⁻¹). This provides the robust foundation for proving the coexistence of Pr³⁺ and Pr⁴⁺ via the reflective–absorptive spectroscopies in the visible-light range.

The XPS data (Figure 6) further indicate the mixed valence of Pr in the atmosphere-based Pr-ZrSiO₄ pigments. As the oxidizing atmosphere is intensified, the ratio of Pr⁴⁺ to Pr³⁺ drastically increases from 0.83 to 1.28, denoting the transcendence of Pr⁴⁺ over Pr³⁺ in amount. This is much distinct from those pigments, like Ca-Pr₂Mo₂O₉,²⁸ in which Pr³⁺ functions dominantly as the primary coloring centers. Additionally, the XRD patterns (Figure S5) of the atmosphere-based pigments indicate that no new crystalline phases appear except the minor phase ZrO₂.

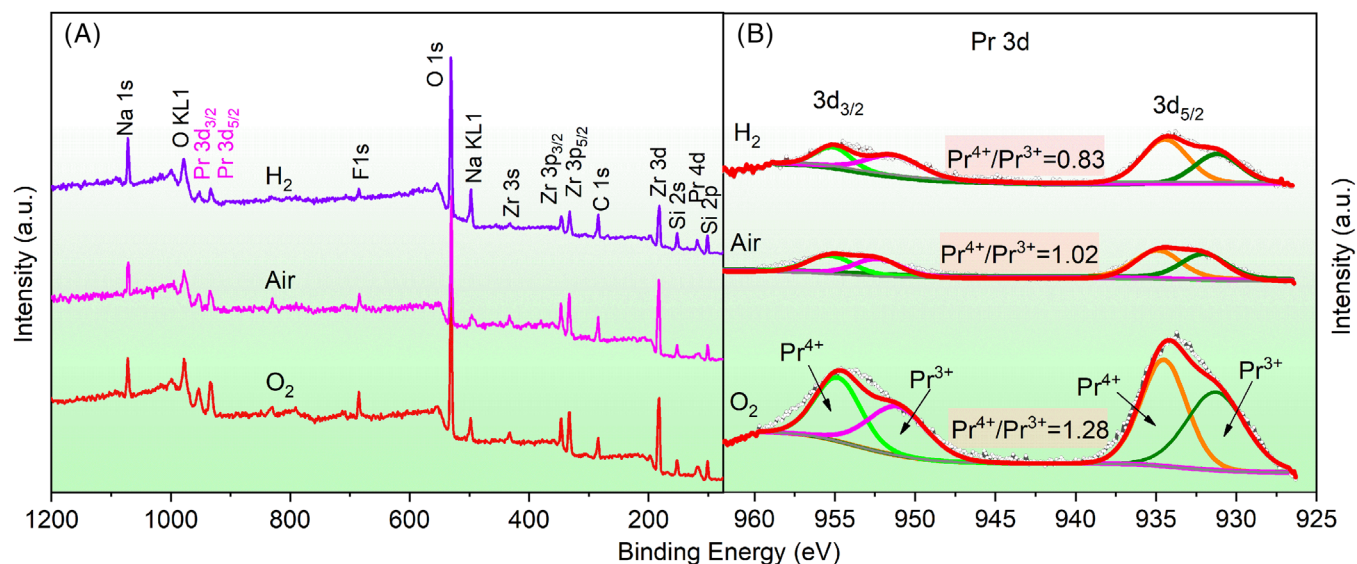


FIGURE 6 (A) Survey X-ray photoelectron spectroscopy (XPS) spectra, and (B) fine XPS spectra for Pr 3d in Pr6 obtained under different atmospheres.

The narrow-band absorption around 591 nm for the transition of ${}^3\text{H}_4 \rightarrow {}^1\text{D}_2$ from Pr^{3+} can reduce the reflectance in the critical yellow-to-orange region at 565–615 nm and hence undermines the yellowish hue. However, the absorption from ${}^3\text{H}_4 \rightarrow {}^1\text{D}_2$ cannot always be observed in many other crystal fields, like Pr-doped CeO_2 pigments,²⁹ in which the absorption from the $4f-5d$ transition and the LMCT band extends over 591 nm and therefore dwarfs the weak absorption from ${}^3\text{H}_4 \rightarrow {}^1\text{D}_2$. Even though this absorption can be occasionally eclipsed in the reflection or absorption spectra, the luminescence of Pr^{3+} can still reveal the existence of the trivalent Pr, as demonstrated in the red-orange pigments of Pr/Fe-Y₂Z₂O₇.¹² The second undesirable absorption by approximately 4%–7% in the H₂-based Pr-ZrSiO₄ pigments extends widely within the green-to-red high-reflectance region above 520 nm (the shade area in Figure 5(B)), which originates most probably from the nonradiative $4f-5d$ transition of the electron-rich Pr^{3+} in the trivalency-dominant pigments (Figure 6(B)). The wide absorption can be neglected by researchers, and it is very likely to be interfered by some uncertain factors, such as a suboptimal control of the calcination temperature and fickle particle sizes for nonconsistent light scattering. This wide absorption can also be observed in many Pr^{3+} -involved inorganic materials, such as the Y₃Al₅O₁₂: $\text{Pr}^{3+}/\text{Ce}^{3+}$ phosphors.³⁰ The deleterious dual absorptions above appreciably impair the chroma of the pigments and should not be ignored.

Excitation and emission spectra (PLE and PL) of the pigments are further presented in Figure 7. As the atmosphere changes from the oxidizing O₂ to the reducing H₂, the characteristic emissive peaks of ${}^3\text{P}_{2,1,0} \rightarrow {}^3\text{H}_4$ from

Pr^{3+} around 440–492 nm, ${}^1\text{D}_2 \rightarrow {}^3\text{H}_4$ at 596 nm, ${}^3\text{P}_0 \rightarrow {}^3\text{H}_6$ at 622 nm, and ${}^3\text{P}_0 \rightarrow {}^3\text{F}_4$ at 718 nm are simultaneously intensified; the variation is consistent with the implications through the UV spectra in Figure 5 and the XPS data in Figure 6. The dominant emissive peak at 622 nm endows the H₂-based pigments with the most brilliant red photoluminescence with excitation at 365 nm; in contrast, the air-based pigments give only a very dim red light (cannot be vividly shown in the image, [Figure 8D–F]), whereas the O₂-based pigments exhibit no visible luminescence due to their lowest content of Pr^{3+} . However, the excitation and emission from Pr^{3+} , even in the O₂-based pigments, can still be detected by the spectrophotometer, indicating the inextricable coexistence of Pr^{3+} and Pr^{4+} in all of these Pr-contained pigments. The three types of pigments give the daylight hues from yellow, to pale yellow and finally to nearly white as the atmosphere varies from oxidizing to reducing (Figure 8A–C). Some additional Pr6 pigments obtained in an inert N₂ atmosphere give very similar light reflection, absorption, luminescence strength, and also daylight yellow color with the air-based pigments (Figures S6 and S7). As a mention, all the pigments cannot be designated as fluorescent pigments: although part of their excitation region at 446–492 nm is just within the visible-light range, the absolute luminescent efficiency around 580–630 nm exceeds no more than 1% (Figure S8, much lower than the high reflectance over 80% and only comparable with the testing uncertainty of usually 1%–2%), and hence the luminescence gives almost no concrete contribution to the visual hue in daylight.

Wide-range absorption spectra at 200–1200 nm for the Pr-ZrSiO₄ pigments and the band structures via the DFT

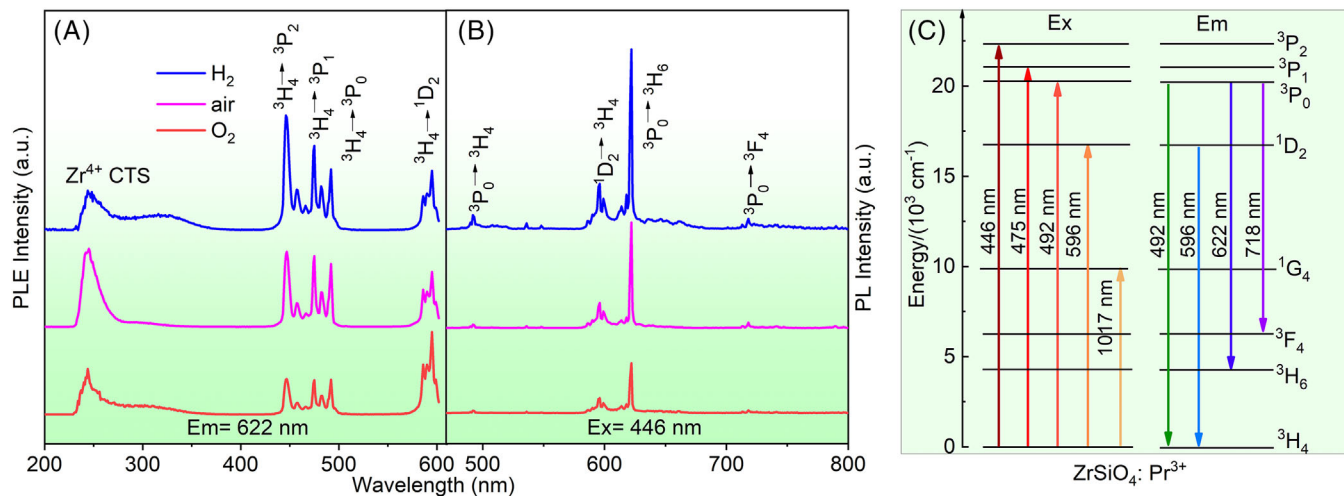


FIGURE 7 (A) Excitation spectra, and (B) emission spectra of Pr6 obtained under different atmospheres; (C) the energy level diagram of Pr³⁺ ions.



FIGURE 8 Macroscopic appearance of the different Pr6 pigments, (A, B, and C) in daylight and (D, E, and F) activated by a 365-nm UV lamp in dark; (A and D) H₂-based, (B and E) air-based, (C and F) O₂-based.

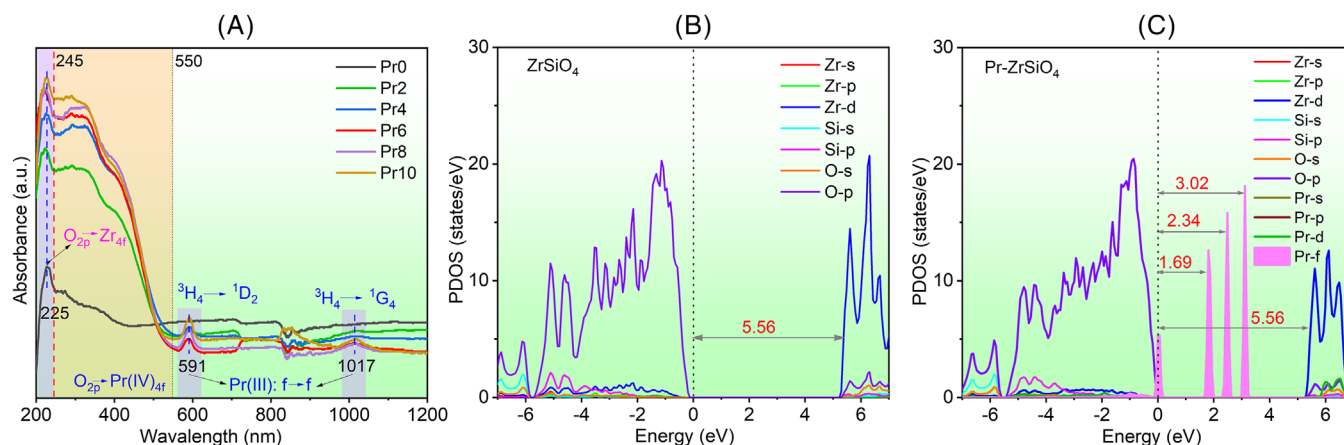


FIGURE 9 (A) Extended absorption spectra at 200–1200 nm for Pr0–Pr10, and partial density of states (PDOS) for (A) pure ZrSiO₄ and (B) the Pr-ZrSiO₄ pigments.

calculation are presented in Figure 9. The band gap of ZrSiO_4 is calculated at 5.56 eV, roughly consistent with the previously calculated or experimental data (5.8–6.0 eV),¹⁵ and it corresponds well with the absorption peak at 225 nm for the LMCT from O_{2p} to Zr_{4d} . When Pr^{4+} is introduced, some intermediate energy levels emerge within the band gap and the wide LMCT from O_{2p} to Pr(IV)_{4f} thus produces sharp photon absorptions below 3.02 eV (particularly above 2.2 eV, the onset energy for green lights at ~560 nm). When the violet–blue lights are sufficiently absorbed, the pigments are rendered with a complementary brilliant yellowish hue. As a mention, zinc is not found in the optimized pigments (Figure S9), and it exerts no influence upon the morphology of final pigments (Figures S10) and S11) and probably promotes more praseodymium into the zircon matrix just as the mineralizer NaF does.

4 | CONCLUSIONS

(1) Both the cations of Pr^{4+} and Pr^{3+} coexist competitively and invariably in all the ultrafine Pr-ZrSiO_4 pigments. An oxidizing atmosphere cannot completely eradicate the Pr^{3+} cations, and a reducing atmosphere is either unable to fully eliminate Pr^{4+} in the Pr-ZrSiO_4 system.

(2) The yellow hue of Pr-ZrSiO_4 pigments originates primarily from the strong wide-band absorption of the LMCT from O_{2p} to Pr(IV)_{4f} . The competitive presence of Pr^{3+} is, however, inclined to discolor the pigments, due to its reduction in the Pr^{4+} content, an evident undesirable narrow-band absorption around 591 nm, and still possibly a wide absorption band in the green-to-red region from the $4f-5d$ transition.

(3) A high-content fluorine in the acidic precursors can be sufficiently incorporated into the hydroxylated zirconium species and hence inhibits the excessive extension of Zr-O-Si networks, thereby generating the Pr-ZrSiO_4 pigments with a well-defined morphology and a desirable submicron dimension with D_{50} ranging 250–400 nm and $\text{IQR} < 80$ nm. An oxidizing atmosphere can significantly promote the content of Pr^{4+} and it, therefore, enhances chromaticity of the yellow pigments.

ACKNOWLEDGMENTS

Our work is financially supported by the National Natural Science Foundation of China, (grant numbers: 51602096, 12174092, 11874144, and 21801071), China Postdoctoral Science Foundation, (grant number: 2020M682382), Hubei Provincial Department of Science and Technology (grant numbers: 2018CFA026 and 2019CFA079), Wuhan Science and Technology Bureau (grant number: 2018010401011268), and the Program of Introducing

Talents of Discipline to Universities (grant number: “111 Project”, D18025).

ORCID

Binglong Lei  <https://orcid.org/0000-0002-1388-7558>

REFERENCES

1. Molinari C, Conte S, Zanelli C, Ardit M, Cruciani G, Dondi M. Ceramic pigments and dyes beyond the inkjet revolution: from technological requirements to constraints in colorant design. *Ceram Int*. 2020, 46(14):21839–72.
2. Chen T, Zha JR, Zhang XJ, Hu XB, Jiang WH, Xie ZX, et al. Synthesis and characterization of $\text{Pr}_x\text{Zr}_{1-x}\text{SiO}_4$ ($x = 0-0.08$) yellow pigments via non-hydrolytic sol-gel method. *J Eur Ceram Soc*. 2018, 38(13):4568–75.
3. Wang Y, Lai F, Wang Q, Long Q, Wang C, Zhang W, et al. Synthesis and chromatic properties of high color performance $\text{Pr}_x\text{-ZrSiO}_4$ ($x = 0-0.1$) yellow pigment. *J Alloy Compd*. 2022, 891:161932.
4. Rivera-Yerena HH, Louvier-Hernández JF, García-Rodríguez FJ, Medrano LS, Pérez E, Patiño-Herrera R. Approaching the most intense reddish yellow tone of praseodymium doped zircon pigment. *J Solid State Chem*. 2021, 297:122084.
5. Wang Q, Wang Y, Chang Q, Liu H, Yang Y, Zhang X. Preparation of ultrafine spherical Pr-ZrSiO_4 pigment by sol-gel-microemulsion method. *Silicon*. 2020, 12(3):585–94.
6. Snyders E, Potgieter JH, Nel JT. The effect of milling and percentage dissociation of plasma dissociated zircon on the colour of Pr-yellow and V-blue zircon pigments. *J Eur Ceram Soc*. 2006, 26(9):1599–603.
7. Wang X, Mu B, Xu J, Wang A. Preparation of high-performance bismuth yellow hybrid pigments by doping with inorganic oxides. *Powder Technol*. 2020, 373:411–20.
8. Dolić SD, Jovanović DJ, Štrbac D, Far LÐ, Dramićanin MD. Improved coloristic properties and high NIR reflectance of environment-friendly yellow pigments based on bismuth vanadate. *Ceram Int*. 2018, 44(18):22731–7.
9. Wendusu HT, Masui T, Imanaka N. Novel environmentally friendly (Bi, Ca, Zn, La) VO_4 inorganic yellow pigments. *RSC Adv*. 2013, 3(47):24941–5.
10. Comstock MC. Complex inorganic colored pigments: comparison of options and relative properties when faced with elemental restrictions. In: *The 56th SCAA Conference*; September 2016; Melbourne VIC, Australia.
11. Kar JK, Stevens R, Bowen CR. Processing and characterisation of Pr-zircon pigment powder. *Adv Appl Ceram*. 2013, 104(5):233–8.
12. Jovaní M, Fortuño-Morte M, Beltrán-Mir H, Cordoncillo E. Environmental-friendly red-orange ceramic pigment based on Pr and Fe co-doped $\text{Y}_2\text{Zr}_2\text{O}_7$. *J Eur Ceram Soc*. 2018, 38(4):2210–7.
13. Liu H-G, Zheng W-C, Yang W-Q. Spin-Hamiltonian parameters and defect structure for tetragonal Pr^{4+} centers in ZrSiO_4 crystal. *Phys B: Condens Matter*. 2009, 404(12):1806–8.
14. Montoya N, Herrera G, Alarcón J. Synthesis and characterization of praseodymium-containing ZrSiO_4 solid solutions from gels. *Ceram Int*. 2011, 37(8):3609–16.

15. Obukuro Y, Matsushima S. First-principles energy band calculation of Pr-doped ZrSiO₄. *J Ceram Soc Jpn.* 2021, 129(12):764–9.
16. Guo DZ, Xie MG, Ma N, Yang Q, Luo ZK, Chu YH, et al. Synthesis and characterization of (Pr, Ce)-ZrSiO₄ ceramic pigments: the properties of the pigments and the effect of Ce. *J Am Ceram Soc.* 2018, 102:2619–28.
17. Guo DZ, Yang Q, Chen PC, Chu YH, Zhang Y, Rao PG. The influence of micronization on the properties of Pr-ZrSiO₄ pigment. *Dyes Pigm.* 2018, 153:74–83.
18. Güngör GL, Kara A, Blossi M, Gardini D, Guarini G, Zanelli C, et al. Micronizing ceramic pigments for inkjet printing: part I. Grindability and particle size distribution. *Ceram Int.* 2015, 41(5):6498–506.
19. Lei BL, Qin W, Kang GL, Peng C, Wu JQ. Modeling and evaluation for encapsulation efficiency of zircon-based heteromorphous encapsulation pigments. *Dyes Pigm.* 2015, 112:245–54.
20. Peng S, Yang H, Chen ZQ, Huang Q, Xia XH, Wang Z. Effect of halide mineralizers on monodisperse spherical zircon powders. *J Am Ceram Soc.* 2021, 104(6):2849–59.
21. Peng S, Chen ZQ, Huang Q, Xia XH, Wang Z, Huang ZB, et al. Manipulation of Lewis acid–base complexation in the Zr-centered quaternary system for monodisperse spherical zircons. *Ceram Int.* 2021, 47(8):10819–27.
22. Cao KW, Guo XH, Gao YF, Luo HJ. Synthesis and characterization of Pr-ZrSiO₄ pigment by a two-step method (in Chinese). *J Inorg Mater.* 2012, 27(9):984–90.
23. Badenes JA, Vicent JB, Llusar M, Tena MA, Monros G. The nature of Pr-ZrSiO₄ yellow ceramic pigment. *J Mater Sci.* 2002, 37:1413–20.
24. Lee JH, Kim YJ. Luminescent properties of Pr doped ZrSiO₄ phosphors. *Ceram Int.* 2008, 34(4):1113–6.
25. Liu W, Zhang Q. Growth and spectral properties of Pr³⁺-doped Y₃Al₅O₁₂ crystal for potential use in all-solidstate visible laser. *Mater Res Innov.* 2017, 21(2):65–8.
26. Zhang F, Bi Z, Huang A, Xiao Z. Luminescence and Judd–Ofelt analysis of the Pr³⁺ doped fluorotellurite glass. *J Lumin.* 2015, 160:85–9.
27. Kasprócz D, Brik MG, Jaroszewski K, Pedzinski T, Bursa B, Głuchowski P, et al. Spectroscopic properties of Bi₂ZnOB₂O₆ single crystals doped with Pr³⁺ ions: absorption and luminescence investigations. *Opt Mater.* 2015, 47:428–34.
28. George G, Kumari LS, Vishnu V, Ananthakumar S, Reddy M. Synthesis and characterization of environmentally benign calcium-doped Pr₂Mo₂O₉ pigments: applications in coloring of plastics. *J Solid State Chem.* 2008, 181(3):487–92.
29. Gonzaga LA, Santana VT, Bernardi MIB, Hrubý J, Neugebauer P, Mesquita A. CeO₂ and CeO₂: Pr nanocrystalline powders prepared by the polymeric precursor method: yellow and red pigments with tunable color. *J Am Ceram Soc.* 2020, 103(11):6280–8.
30. Yong D, Chong-Yun S, Yong-Jun D, Qiu-Hong Y, Wei H. Spectral investigation of R, Ce: YAG (R: Pr³⁺, Eu³⁺, Gd³⁺) single crystals and their applications in white LEDs. *Chin Phys B.* 2015, 24(11):117801.

SUPPORTING INFORMATION

Additional supporting information can be found online in the Supporting Information section at the end of this article.

How to cite this article: Peng S, Yang R, Lei B, Chen R, Gao Y, Xia X, et al. New insight into the coloration mechanism and synthesis of ultrafine Pr-ZrSiO₄ yellow pigments. *J Am Ceram Soc.* 2023;1–11. <https://doi.org/10.1111/jace.19150>